

**DEFECT DETECTION AND CLASSIFICATION OF
SILICON SOLAR WAFER FEATURING NIR IMAGING
AND IMPROVED NIBLACK SEGMENTATION**

ZEINAB MAHDAVIPOUR

UNIVERSITI SAINS MALAYSIA

2016

**DEFECT DETECTION AND CLASSIFICATION OF SILICON SOLAR
WAFER FEATURING NIR IMAGING AND IMPROVED NIBLACK
SEGMENTATION**

by

ZEINAB MAHDAVIPOUR

**Thesis submitted in fulfillment of the requirements
for the degree of
Doctor of Philosophy**

April 2016

ACKNOWLEDGEMENT

I wish to express my profound gratitude to God Almighty for His protection. I would like to appreciate my supervisor, Prof. Mohd Zaid Abdullah who has inspired and accompanied me throughout this study. His constant guidance, subjective criticism, continuous support, and great inspiration throughout the duration of my study are most valued. It is a great opportunity and honour to have worked under his supervision.

I would like to extend my heartiest appreciation to the Institute of Postgraduate Studies (IPS), Universiti Sains Malaysia for their contribution to this research through the Collaborative Research in Engineering, Science and Technology (CREST) grant304/PELECT/6050264/C121. I would also like to thank our industrial partner TT-Vision Technologies for partly sponsoring this project.

Special thanks go to the School Electrical and Electronic Engineering, USM for providing the necessary facilities and equipment. My sincere thanks go to all administrative and technical staff in the School, particularly Pn. Normala, En. Rahmat, Pn. Khalijah, En. Nor Azhar, En. Amir Hamid, and En. Naim. They offered instant assistance whenever needed. I would like to thank my colleagues and friends who provided encouragement and help.

Last but not least, I express my deepest respect and appreciation to my beloved husband and parents for their kindness, support, patience, and encouragement throughout my study. I will always be indebted to them. I sincerely thank you all for your understanding, trust, encouragement, and faith during the years of my study. Without their encouragement and love, this work could not have been completed.

TABLE OF CONTENTS

Acknowledgement	ii
Table of Contents.....	iii
List of Tables.....	vi
List of Figures.....	vii
List of abbreviations.....	xi
List of Symbols.....	xiii
Abstrak.....	xv
Abstract.....	xvii

CHAPTER 1- INTRODUCTION

1.1 Motivation	1
1.2 Problem Statement	4
1.3 Scope and Research Objectives	8
1.4 Thesis Outline	9

CHAPTER 2 - REVIEW OF LITERATURE

2.1 Introduction	10
2.2 Crack and Defect Detection Algorithms	10
2.3 Image Thresholding	16
2.3.1 Niblack Thresholding.....	17
2.3.2 Segmentation Methods.....	25
2.3.2.1 Sobel Technique.....	25
2.3.2.2 Canny Technique.....	26
2.3.2.3 Otsu Technique.....	27
2.3.2.4 Anisotropic Diffusion Technique.....	28
2.4 Feature Extraction	32
2.5 Machine Learning	40
2.5.1 Support Vector Machines	43
2.5.2 Multi-class SVM	47
2.5.2.1 One-Versus-All (OVA) Method	48
2.5.3 Unsupervised Classification.....	49

2.6 Summary 54

CHAPTER 3 - METHODOLOGY

3.1 Introduction 55

3.2 Defect Inspection 56

 3.2.1 Sample Dataset 57

 3.2.2 Optical Setup..... 57

3.3 Image Segmentation 66

 3.3.1 Adaptive Thresholding Methods 67

 3.3.1.1 Niblack’s Segmentation 68

 3.3.1.2 Proposed Method 1..... 68

 3.3.1.3 Proposed Method 2..... 70

 3.3.1.4 Filtering 72

 3.3.1.5 Experimental Procedure 73

 3.3.2 Performance Evaluation 73

 3.3.2.1 Confusion Matrix 74

 3.3.2.2 Sensitivity and Specificity 75

 3.3.2.3 Pratt’s Figure of Merit 77

3.4 Defect Feature 77

3.5 Classification 79

 3.5.1 Defect Classification 80

 3.5.2 Experimental Procedure 81

 3.5.3 Accuracy Measures of Clustering 85

 3.5.3.1 Rand Index 85

 3.5.3.2 Silhouette Index 85

3.6 Summary 86

CHAPTER 4 - EXPERIMENTAL RESULTS

4.1 Introduction 87

4.2 Image Processing..... 87

 4.2.1 Threshold Results 1 88

 4.2.1.1 Quantitative Evaluation 96

4.2.2 Threshold Results 2.....	104
4.2.2.1 Quantitative Evaluation.....	111
4.3 Classifiers Analysis	118
4.4 Summary	128

CHAPTER 5 - CONCLUSION AND FUTURE WORK

5.1 Conclusion and Research Contributions	129
5.2 Limitation of the Techniques	132
5.3 Suggestions for Future Work	133

REFERENCES	135
-------------------------	-----

APPENDICES

LIST OF PUBLICATIONS

LIST OF TABLES

	Page
Table 3.1 The image datasets	57
Table 3.2 An instance of a confusion matrix with incorrectly and correctly classified categories for 10 samples, here, “ \boxplus ” signifies correctly classified and “ \boxminus ” signifies incorrectly classified	74
Table 3.3 Typical confusion matrix for a binary classifier or detection	75
Table 4.1 The z and k values computed from Figure 4.1	90
Table 4.2 The edge evaluation results averaged using 100 samples comparing several thresholding techniques with the proposed method	103
Table 4.3 The quantitative evaluation results calculated from (a) polycrystalline and (b) monocrystalline solar wafer samples. In each case the quality measures are averaged from 50 samples	113
Table 4.4 Total number of good and imperfect samples	123
Table 4.5 The evaluation result of k -mean clustering	123
Table 4.6 The SVM classification results of Dataset 2	128

LIST OF FIGURES

		Page
Figure 1.1	Examples of polycrystalline solar wafer images: (a) is an intact or good sample, (b) is a micro crack sample; (c) a defective sample that includes fingerprint, and (d) is defected by a Stain. In (b) and (d), the locations of micro-crack and stain are indicated by arrows	3
Figure 2.1	Binarization result: (a) Original image, (b) Niblack's result (Chiou <i>et al.</i> , 2012)	14
Figure 2.2	Binarization result: (a) Original image, (b) Niblack's result (Feng & Tan, 2004)	18
Figure 2.3	Binarization result: (a) Original image, (b) Sauvola & Pietikainen's result (Feng & Tan, 2004)	19
Figure 2.4	Binarization result: (a) Original image, (b) Wolf and Jolion's result (Feng & Tan, 2004)	20
Figure 2.5	Binarization result: (a) Original image, (b) Feng and Tan's result (Feng & Tan, 2004)	21
Figure 2.6	Binarization result: (a) Original image, (b) NICK's result (Bataineh <i>et al.</i> , 2011)	22
Figure 2.7	Binarization result: (a) Original image, (b) Bataineh <i>et al.</i> 's result (Bataineh <i>et al.</i> , 2011)	23
Figure 2.8	Binarization result: (a) Original image, (b) Chiu <i>et al.</i> 's result (Chiu <i>et al.</i> , 2012)	25
Figure 2.9	x-direction (G_x) and y-direction (G_y) for Sobel convolution masks	25
Figure 2.10	Binarization result: (a) Original image, (b) Canny's result (Canny, 1986)	27
Figure 2.11	Binarization result: (a) Original, (b) Otsu	28
Figure 2.12	Binarization result: (a) Original image, (b) Tsai <i>et al.</i> 's result (Tsai <i>et al.</i> , 2010)	31

Figure 2.13	Binarization result: (a) Original image, (b) Anwar and Abdullah's result (Anwar & Abdullah, 2014)	32
Figure 2.14	Example of a contour illustrated by elliptic Fourier descriptors	38
Figure 2.15	SVM utilizes hyperplane margin to divide negative from positive classes	45
Figure 2.16	Example of k -mean algorithm: (a) input data set, (b) three seed points selected as cluster centers, (c) result after second iteration, (d) result after third iteration, (c & d) intermediate iterations updating cluster labels and their centers, and (e) final clustering by k -mean	51
Figure 3.1	Flow chart summarising the defect detection algorithm	56
Figure 3.2	Transmittance of light source with different wavelengths through a solar wafer (Ko <i>et al.</i> , 2013)	59
Figure 3.3	(a) The schematic of backlight illumination, (b) the actual backlight illumination set-up	60
Figure 3.4	(a) The schematic of front-light illumination, (b) the actual front-light illumination system	61
Figure 3.5	The overall hardware set-up of the solar wafer inspector showing the important components	62
Figure 3.6	Examples of polycrystalline solar wafer images produced by the NIR system in Figure 3.5, (a) intact or good sample, (b) defected samples due to (i) micro-crack, (ii) fingerprint, and (iii) stain or glove marks. Dotted circles in (b) show the locations of the defects.	63
Figure 3.7	Examples of polycrystalline and monocrystalline solar wafer images as Dataset 2, (a) and (b) are defective polycrystalline and mono-crystalline samples respectively. The circles indicate the locations of the defect	63
Figure 3.8	(a) stain (b) micro-crack (c) fingerprint as defective samples captured by using front-light and backlight illuminator	64

Figure 3.9	Flowchart of the proposed image thresholding algorithm	67
Figure 3.10	Examples of polycrystalline solar wafer images produced by the NIR system in Figure. 3.6 as dataset 1, (a) is intact or good sample, (b) is micro crack sample; (c) fingerprint, and (d) is defected by stain or glove marks, the circle indicates the location of stain	78
Figure 3.11	Block diagram of defect detection and classification	81
Figure 3.12	Flowchart of k -mean clustering	84
Figure 4.1	Examples of thresholding results (a): Original images which are displayed as: (i) micro crack, (ii) defective images including micro cracks and other invisible defects such as scratches, and (iii) finger print defect. (b) Segmented images without z and k parameters, and (c) proposed segmented incorporating z and k parameters	89
Figure 4.2	Defect detection of NIR images comparing the proposed technique with Sobel (1970), Otsu (1979), Canny (1986), and anisotropic diffusion (Tsai et al., 2010) thresholdings: (a) Sobel, (b) Otsu, (c) Canny, (d) anisotropic diffusion, and (e) the proposed technique	91
Figure 4.3	Segmentation results comparing the proposed and the original Niblack formula including some of its popular variants. (a) input images (b) ground truth images corresponding to images in (a), (c) Niblack (1985), (d) Sauvola and Peitaikanen (2000), (e) Feng and Tan (2004), (f) Wolf and Jolion (2004), (g) Bataine <i>et al.</i> (2011), (h) Chiu <i>et al.</i> (2012), and (i) proposed method	94
Figure 4.4	The average accuracy evaluation results	98
Figure 4.5	The average FOM evaluation results	99
Figure 4.6	The average DSC evaluation results	100
Figure 4.7	The average SEN evaluation results	101
Figure 4.8	The average FNR and FPR evaluation results	102
Figure 4.9	(a) The original images (b) the results without adaptive k , z and x parameters (c) the results of the proposed Method 2	104

Figure 4.10	Examples of thresholding results (a) original images, (i-ii) mono-crystalline, (iii-iv) polycrystalline solar wafers, (b) proposed segmented incorporating z , x and k parameters, (c) Sobel (1970), (d) Otsu (1979), (e) Canny (1986), (f) Diffusion (Tsai <i>et al.</i> , 2010)	105
Figure 4.11	Examples of binarised results comparing the proposed and the original Niblack formula, including its recent variants (a) original images, (b) Niblack (1985), (c) Sauvola and Pietikainen (2000), (d) Bataineh <i>et al.</i> (2011), (e) Chiu <i>et al.</i> (2012), (f) Feng and Tan (2004), (g) Wolf and Jolion (2004), (h) proposed method, and (i) Ground truth images corresponding to images in (a). In all images, (i-ii) are mono-crystalline and (iii-iv) are polycrystalline solar wafers.	108
Figure 4.12	(a) defective images of Dataset 1, (b) results of proposed Method 2 (c) results of proposed Method 1	115
Figure 4.13	(a) the defective images of Dataset 2, (b) the results of proposed Method 1 (c) the results of proposed Method 2	116
Figure 4.14	The normalized $ \overline{EFD} $ of solar wafer images samples: (a) original images, (b) results after thresholding and filtering, (c) results after connected component, (d) boundary results and (e) spectrum of normalized $ \overline{EFD} $	120
Figure 4.15	Elbow chart showing the variation of SSE with k_c	122
Figure 4.16	Elbow chart showing the variation in the performance variance with k_c	123
Figure 4.17	Distribution of clustering results of 2000 samples Dataset 1, comprising of different types of Dataset 1 samples	124
Figure 4.18	Scatter distribution of clustering results on different types of samples	124
Figure 4.19	The Silhouette result of clustering	125
Figure 4.20	The Rand index results of clustering	126
Figure 4.21	The accuracy results of classification	128

LIST OF ABBREVIATIONS

ACC	Accuracy
AFKM	Adaptive fuzzy k-means clustering
AEFD	Average of Elliptic Fourier descriptors
Am	Amplitude
A2DKM	Automated two-dimensional k-Means
ANN	Artificial neural network
BCC	Bandwidth Cluster Center
CCD	Charge-coupled device
DA	Discriminant analysis
DAGSVM	Directed acyclic graph SVM
DSC	Dice similarity coefficient
DWT	Discrete wavelet transform
EFDs	Elliptic Fourier descriptors
EL	Electroluminescence
EM	Elbow method
FA	Factor analysis
FNR	False negative rate
FOM	Pratt's figure of merit
FPR	False Positive Rate
FTA	Focal plane array
FCM	Fuzzy c-means
GK	Gustafson-kessel
HRBF	Hybrid radial basis function
IR-LED	Infrared Light Emitting Diode
L	Level
LR	Linear regression
MATLAB	Matrix laboratory
MDRL	Manifold discriminant regression
	Learning
NIR	Near Infrared
OVA	One-versus-all

PL	Photo luminescence
RBF	Gaussian radial basis function
RHT	Radiant heat thermography
RI	Rand index
RMDRL	Robust manifold discriminant regression learning
RUV	Resonance ultrasonic vibration
SAM	Scanning Acoustic Microscopy
SEN	Sensitivity
SI	Silhouette index
SMO	Sequential minimum optimization
SPE	Specificity
SSE	Sum of square errors
SVM	Support vector machine
SV _s	Support vectors
TN	True negative
TNR	True negative rate
TP	True positive
TPR	True positive rate
WCSS	Within-cluster sum of squares

LIST OF SYMBOLS

a_n, b_n, c_n, d_n	Coefficients to extract features
b	Bias term
B	Magnitude average of EFD threshold image
C	Regularization parameter
c_c	Centre, centroid
dc	Diffusion coefficient
d^*	Degree of polynomial kernel
d, d_{ij}, d_e	Euclidean distance
div	Divergent operator
$f, f_i, f_{ij}, \hat{f}_k$	Classification function
G	Gray-level of an image
I	Input image
\bar{I}	Binarised input image
i, j, m, n	Index variable
K	Kernel function
K^*	Edge stopping threshold
k	Normalisation factor
k_c	Number of cluster
l	Number of samples
l_i	Number of samples in class i
μ	Mean
μ_g	Mean value of the global image pixels
μ_i	Mean of points belonging to each cluster
μ_w	Mean value of the pixels in binarization window
M	Minimum gray value of image
max_{level}	Maximum gray level value
N	Number of Fourier harmonics
N_c	Number of dataset in cluster
N_D	Numbers of detected edge pixels
N_I	Numbers of ideal edge pixels
N_p	Neighbourhood pixels

N	Total number of pixels in an image
p_i	Pixel value
R	Maximum gray-value standard deviation
RS	Dynamic range of standard deviation
σ	Standard deviation
$\sigma_{adaptive}$	Adaptive standard deviation
σ_{max}	Maximum standard deviation
σ_{min}	Minimum standard deviation
σ_w	Window standard deviation
Sm_{ij}	Separability measure between class i and class j
T, T_H, T_L	Threshold
T	Total contour length
t	Iteration
$u, v,$	Index variable
W	Weight vector
X, X_i, X_n	Input feature vector for each sample
\bar{X}_i	Vector of group mean
y_i, y_n^{ij}	Class label (+1 or -1)
z, x, k	Proposed defined parameters
∇	Gradient
δ	Sigma term of the Gaussian kernel function

**PENGESANAN KECACATAN DAN PENGELASAN WAFER SOLAR
SILIKON DENGAN MENGGUNAKAN KAEDAH PENGIMEJAN NIR DAN
SEGMENTASI NIBLACK YANG DITAMBAHBAIK**

ABSTRAK

Menghasilkan tenaga yang boleh diperbaharui berkuantiti tinggi memerlukan kecekapan yang tinggi dalam fabrikasi produk wafer silikon, yang juga merupakan komponen asas panel solar. Oleh yang demikian, pemeriksaan kualiti yang tinggi untuk wafer solar semasa proses pengeluaran sangat penting. Dalam tesis ini, sistem pengesanan kecacatan yang cekap dan automatik menggunakan strategi pengelasan dan kelompok termaju telah dicadangkan. Dalam kajian ini, satu skema mesin penglihatan untuk mengesan keretakan mikro dan kecacatan-kecacatan yang lain dalam pembuatan polihabluran dan mono kristal wafer solar dicadangkan dan dibangunkan. Pemeriksaan retak mikro sangat mencabar kerana kecacatan ini sangat kecil dan tidak boleh dilihat dengan mata kasar. Kewujudan struktur heterogenus yang lain dalam wafer solar seperti bahan-bahan kasar dan kawasan gelap menjadikan pemeriksaan lebih mencabar. Dalam tesis ini, sebuah inspektor retak mikro yang mengandungi pencahayaan inframerah yang dekat dan algoritma segmentasi Niblack yang diperbaharui telah dicadangkan. Keputusan emperikal dan visual menunjukkan ketepatan dan prestasi yang lebih baik dari segi angka merit Pratt dan kaedah penilaian yang lain berbanding dengan formula pengembangan Niblack yang sedia ada. Keputusan angka merit (FOM), ketepatan (ACC), pekali kesamaan dadu (DSC) dan sensitiviti yang masing-masingnya sentiasa lebih tinggi daripada 0.871, 99.35 %, 99.68 %, dan 99.75 % bagi imej-imej dalam kajian ini. Sementara itu, satu set deskriptor bersepadanan dengan penerangan ciri-ciri bentuk Fourier eliptik, diekstrak bagi setiap kecacatan yang telah dikesan, dan dinilai bagi

setiap kluster bagi tujuan pengelompokan dan pengelasan. Pengelasan menggabungkan analisis ciri keamatan kecacatan, penggunaan tanpa pengawasan kelompok purata- k dan pelbagai kelas algoritma SVM. Kaedah-kaedah ini telah digunakan untuk pengesanan, pengelompokan dan klasifikasi imej wafer solar polihabluran, bersepadanan dengan kecacatan seperti keretakan mikro, kekotoran, dan cap jari. Keputusan kajian menunjukkan bahawa kaedah purata- k dan penklasifikasi SVM mampu mengelompok dengan tepat kecacatan-kecacatan tersebut dengan ketepatan, indeks Rand, dan Bayang indeks dengan nilai purata masing-masing sebanyak 99.8 %, 99.788 %, dan 98.43 %.

DEFECT DETECTION AND CLASSIFICATION OF SILICON SOLAR WAFER FEATURING NIR IMAGING AND IMPROVED NIBLACK SEGMENTATION

ABSTRACT

Producing a high yield of renewable energy requires a high efficiency in product fabrication of silicon wafers, which is the basic building component of solar panels. For this reason, the high quality inspection of solar wafers during the procedures of production is very important. In this thesis, an automatic and efficient defect detection system, utilising advanced classification and clustering strategies are proposed. In this study a machine vision scheme for detecting micro-cracks and other defects in polycrystalline and monocrystalline solar wafer manufacturing is proposed and developed. Micro-crack inspection is very challenging, because this type of defect is very small and completely invisible to the naked eye. The presence of other heterogeneous structures in solar wafers like grainy materials and dark regions further complicates the problem. In this study an efficient micro-crack inspector comprising near infrared illumination and an improved Niblack segmentation algorithm is proposed. Empirical and visual results demonstrate that the proposed solutions are competitive when compared to existing Niblack thresholding formulas and other standard methods, and achieve better precision and performance in terms of Pratt's figure of merit and other evaluation methods. Result in a figure of merit (FOM), accuracy (ACC), dice similarity coefficient (DSC), and sensitivity were consistently higher than 0.871, 99.35 %, 99.68 %, and 99.75 %, respectively, for all images tested in this study. Meanwhile, a set of descriptors corresponding to Elliptic Fourier Features shape description is extracted for each defect and is evaluated for

each cluster to use for clustering and classification part. The classification combines the analysis of defect intensity features, the application of unsupervised *k*-mean clustering and multi-class SVM algorithms. The methods have been applied for detecting, clustering and classification polycrystalline solar wafer images, corresponding to defects such as micro cracks, stain, and fingerprints. Results indicate that the *k*-mean and SVM classifier can accurately cluster the defects with accuracy, Rand index, and Silhouette index averaging at 99.8 %, 99.788 %, and 98.43 %, respectively.

CHAPTER 1

INTRODUCTION

1.1 Motivation

The increasing demand for renewable energy has led to the growth in the production of solar cells and wafers. Naturally, there has also been an increase in silicon wafer production, which forms the basic building component of many solar panels. According to the statistics published by the Silicon Manufacturer Groups, the worldwide shipments of solar wafers achieved a record high of 2,587 millions square inches shipped in the second quarter of 2014 (Calif, 2014). Depending on the materials used in the manufacturing, solar wafers and cells can be divided into two major types. They are (i) monocrystalline wafers, which are utilized in the manufacture of integrated circuits and transistors, and (ii) polycrystalline silicon wafers, which are commonly utilized in solar power and semiconductor industries (Sparenberg, 2009). In industrial applications, polycrystalline wafers are the preferred material in the production of solar wafers due to lower manufacturing costs (Tsai *et al.*, 2010; Belyaev *et al.*, 2006). However, the imperfection of manufacturing processes has led to a substantial reduction in production yields. Around 5 %-10 % of the total numbers of wafers produced are defective, which in turn causes energy wastage due to increases production costs (Chiou *et al.*, 2011; Rupnowski & Sopori, 2009). Thus, one of the most important procedures in the production of solar wafers is the inspection defects. Chief among these defects are micro-cracks, which contribute to stress fractures and thus equipment down time. The problem is very challenging because this type of defect is very small and completely invisible to the naked eye, which is formed inside the solar wafer and can only be visualised electronically or sensed mechanically. Depending on its size, the micro-cracks

can be categorised into two groups. The first group comprises micro-cracks with sizes less than $30\ \mu\text{m}$, while the second group comprises those at bigger than $30\ \mu\text{m}$ in size (Chiou *et al.*, 2011; Israil *et al.*, 2013). Moreover, the presence of other heterogeneities in the solar wafer, such as grainy material or broken metal fingers, can cause the wafer images to be highly textured with a densely heterogeneous background when visualised electronically. The low contrast between intact and defective pixels further complicates the problem. Traditionally, the near infrared (NIR) spectrum has been used for the purpose of imaging, since this type of radiation is transparent to most of the materials which make-up solar wafers. Compared to other imaging techniques, NIR offers advantages in terms of high accuracy, good sensitivity and faster response time (Israil *et al.*, 2013). However, NIR imaging requires very powerful and advanced image processing techniques, since the image that it produces usually contains many artefacts.

Examples of polycrystalline solar wafer images, which include an intact sample and several other samples that possess such imperfections as micro cracks, stains, and fingerprints, are shown in Figure 1.1. In reality there are other types of defects in solar wafers products but the common defects as micro crack, fingerprint and stain are shown in this figure. In order to solve this kind of multi-class problem found within photovoltaic industry, several methods have been used.

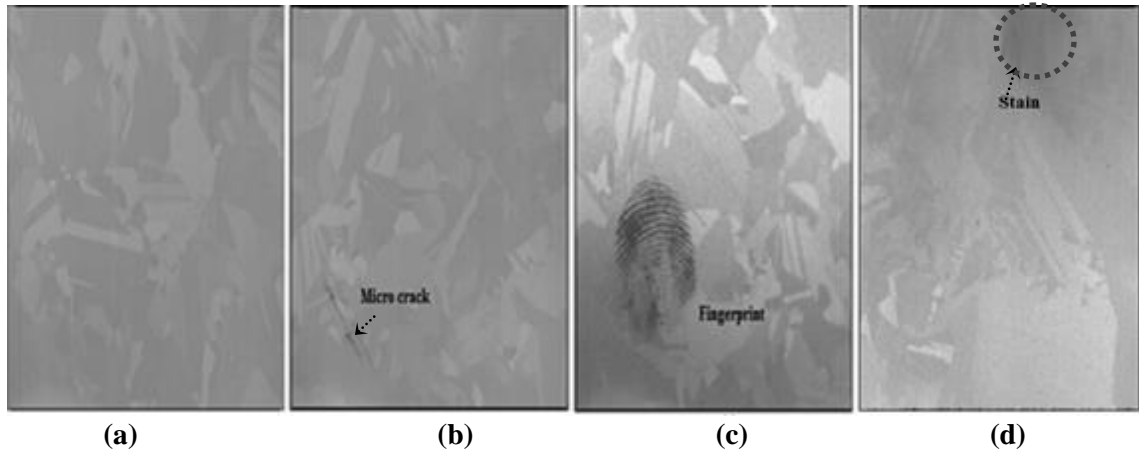


Figure 1.1: Examples of polycrystalline solar wafer images Dataset 1: (a) is an intact or good sample, (b) is a micro crack sample; (c) a defective sample that includes fingerprint, and (d) is defected by a stain. In (b) and (d), the locations of micro-crack and stain are indicated by arrows.

In the recent years, there has been an increasing trend in the use of machine vision in the manufacturing sectors and industry. This includes methods used to supply imaging-based automatic inspection and analysis for applications such as automatic inspection, process control, and robot guidance in industry. Typical tasks of machine vision in the industrial vision inspection system include: image acquisition, image processing, feature extraction, and decision making (Malamas *et al.*, 2003). The use of machine vision in industrial automation provides a better solution, as it helps to increase productivity and quality through consistent, accurate and fast inspection. However, due to the lack of image processing and artificial intelligence algorithms which are suitable and accurate in solving the inspection tasks involved, the inspection and grading processes continue to be manual or semi-manual efforts (Anwar, 2014). Inevitably, the problem of detecting defects in solar wafer also exhibit similar circumstances. Conventionally, the solar wafers consist of invisible and visible defects. The main defects as the invisible defects are micro-cracks and the visible defects are stains,

fingerprints. Because of the increasing of using solar cells and wafer applications, even the defects that do not directly link to reliability issues such as water mark and surface stain, fingerprint are detected and considered as fail or secondary grade of cells for the solar cell and wafer buyers. Those defects are visually inspected by operators. However, the inconsistent inspection results caused by human error make the fully automatic optical inspection solution become essential equipment for crystalline cell and wafer products (Chroma, 2015).

Therefore, there is a research prospective, specifically in the field of machine vision, to solve the problem of micro-cracks and the detection of other defects and classifications in solar wafers. Motivated by this need, this thesis presents the methods and techniques for detecting defects in the images of polycrystalline and monocrystalline solar wafers. This study integrates an image-processing and machine-learning platform toward an application in invisible and visible defect inspection and classification. It addresses image processing techniques based on an adaptive Niblack filter and its application in solar wafer images. Additionally, this work examines the EFD method for feature extraction. Furthermore, machine learning and classification based on unsupervised clustering is investigated. For the sake of completeness this work also examines the classification based on multiclass supervised support vector machines (SVM).

1.2 Problem Statement

Among the tests that need to be carried out on solar wafers includes the inspection of micro-cracks and other defects such as stains and fingerprint. In an effort to reduce the cost of production, manufacturers are making increasingly thinner solar wafers. Though cheaper to produce, such products suffer from a serious drawback, in

that they are relatively more fragile and hence easily broken if not handled properly. Moreover, the thinner the wafer, the greater the chances of forming micro-cracks and other defects. On average, about 5 to 10 percent of solar wafers tend to break during production (Rupnowski & Sopori, 2009). It is important that these micro-cracks and other defects are detected and extracted as early as possible to minimise machine outages or other complications resulting from processing defected samples, especially during assembly or packaging.

There are various methods which can be used in the detection of micro-cracks and other defects. Among them are Radiant Heat Thermography (RHT) (Devitt *et al.*, 1992; Pilla *et al.*, 2002), eddy currents (Johnson & Esquivel, 2006; Zenzinger *et al.*, 2007), dye inspection (Zenzinger *et al.*, 2007), the ultrasonic method (Reber & Beller, 2003), the Scanning Acoustic Microscopy Method (SAM) (Knauss *et al.*, 1995; Connor *et al.*, 1998), Resonance Ultrasonic Vibration (RUV) (Dallas *et al.*, 2008; Polupan, & Ostapenko, 2006), optical transmission (Ko *et al.*, 2013; Abdelhamid *et al.*, 2014), Photo Luminescence (PL) (Chiou *et al.*, 2011; Trupke *et al.*, 2006a; Trupke *et al.*, 2006), Electro Luminescence (EL) (Takahashi *et al.*, 2006; Dreckschmidt *et al.*, 2007; Tsai *et al.*, 2012; Anwar & Abdullah, 2014), and infrared thermography (Pilla *et al.*, 2002).

Some of these methods, especially infrared thermography and RHT, are less popular because of their limited capability in distinguishing micro-cracks from other textures in a solar wafer image. Meanwhile, methods like dye mapping and RUV have limited use because they can potentially damage the sample during inspection.

In contrast, EL does not suffer from the same problems as mechanical methods, since it is a completely non-destructive inspection technique. However, this method